Edge states in topological magnon insulators

Alexander Mook,[1] Jürgen Henk,[2] and Ingrid Mertig[1,2]
[1]*Max-Planck-Institut für Mikrostrukturphysik, D-06120 Halle (Saale), Germany*
[2]*Institut für Physik, Martin-Luther-Universität Halle-Wittenberg, D-06099 Halle (Saale), Germany*
(Received 15 May 2014; revised manuscript received 27 June 2014; published 18 July 2014)

For magnons, the Dzyaloshinskii-Moriya interaction accounts for spin-orbit interaction and causes a nontrivial topology that allows for topological magnon insulators. In this theoretical investigation we present the bulk-boundary correspondence for magnonic kagome lattices by studying the edge magnons calculated by a Green function renormalization technique. Our analysis explains the sign of the transverse thermal conductivity of the magnon Hall effect in terms of topological edge modes and their propagation direction. The hybridization of topologically trivial with nontrivial edge modes enlarges the period in reciprocal space of the latter, which is explained by the topology of the involved modes.

DOI: 10.1103/PhysRevB.90.024412 PACS number(s): 66.70.−f, 75.30.−m, 75.47.−m, 85.75.−d

I. INTRODUCTION

Understanding the physics of electronic topological insulators has developed enormously over the past 30 years: spin-orbit interaction induces band inversions and, thus, yields nonzero topological invariants as well as edge states that are protected by symmetry [1–3]. During this development the concept of Berry curvature [4] and Chern numbers has arisen in various contexts and laws of condensed matter physics. This led for example to the formulation of the bulk-boundary correspondence [5]. Topological arguments and concepts—gained mostly from studies of electronic systems [6]—are applicable to phononic and magnonic systems as well: the phonon Hall effect [7] was successfully explained in terms of Berry curvature and topology [8,9].

Recently, the magnon Hall effect (MHE) was discovered in the insulating ferromagnet $Lu_2V_2O_7$ with pyrochlore lattice structure [10]. The transverse heat current upon application of a longitudinal temperature gradient was explained by uncompensated net magnon edge currents that are mathematically described in terms of the Berry curvature [11,12]. The edge currents originate from the topology of the "topological magnon insulator" [13]. The nontrivial topology is brought about by the spin-orbit interaction which manifests itself as Dzyaloshinskii-Moriya (DM) contribution to the exchange interaction of localized magnetic moments. The Dzyaloshinskii-Moriya interaction shows up in systems without inversion center—as is the case in the aforementioned pyrochlore lattice or in its two-dimensional counterpart, the kagome lattice (Fig. 1).

The rich topology of the kagome lattice not only puts forward itself for an investigation of the bulk-boundary correspondence but also affects crucially the magnon Hall effect. Therefore, a detailed understanding of the MHE in the kagome lattice is a prerequisite for investigations of pyrochlore lattices, such as $Lu_2V_2O_7$.

In this paper, we report on such a study. We focus on two topological phases in which the sign of the transverse thermal conductivity—and hence the direction of the resulting heat current—is unique [14]. We explicitly show the correspondence of thermal Hall conductivity with the propagation direction of the nontrivial edge states. Furthermore, we establish that hybridization of topologically trivial with nontrivial edge modes causes a doubling of the period of the latter in reciprocal space.

The paper is organized as follows. In Sec. II we sketch the quantum-mechanical description of magnons in kagome lattices (Sec. II A), Berry curvature and Chern number (Sec. II B), and the Green function renormalization method for calculating edge states in semi-infinite systems (Sec. II C). Results are presented in Sec. III: edge states of the semi-infinite kagome lattice for different edges and different topological phases (Sec. III A), the connection between the edge modes and the sign of the thermal Hall conductivity (Sec. III B), as well as the hybridization of topologically trivial and nontrivial edge states (Sec. III C). An outlook is given in Sec. IV.

II. THEORY

A. Model Hamiltonian for magnons in a kagome lattice

A two-dimensional kagome lattice is composed of a three-atomic basis which is arranged at the corners of an equilateral triangle with side length equal to half of the lattice constant a (Fig. 1). The lattice vectors read

$$\boldsymbol{a}_1 = \frac{a}{2}(\boldsymbol{x} + \sqrt{3}\boldsymbol{y}), \tag{1a}$$

$$\boldsymbol{a}_2 = \frac{a}{2}(-\boldsymbol{x} + \sqrt{3}\boldsymbol{y}) \tag{1b}$$

in Cartesian coordinates.

Magnons in the kagome lattice are described by a quantum-mechanical Heisenberg model [15] with Hamiltonian

$$\mathcal{H} = \mathcal{H}_{\mathrm{H}} + \mathcal{H}_{\mathrm{DM}} + \mathcal{H}_{\mathrm{ext}}. \tag{2}$$

In the isotropic symmetric spin-spin interaction, i.e., the Heisenberg exchange

$$\mathcal{H}_{\mathrm{H}} = -\sum_{n\neq m} J_m^n \hat{\boldsymbol{s}}_m \cdot \hat{\boldsymbol{s}}_n, \tag{3}$$

two spin operators $\hat{\boldsymbol{s}}_m$ and $\hat{\boldsymbol{s}}_n$ at sites n and m are coupled by symmetric exchange parameters $J_m^n = J_n^m$. The eigenvectors

$$|\boldsymbol{k}\rangle = \frac{1}{\sqrt{N}} \sum_m \mathrm{e}^{\mathrm{i}\boldsymbol{k}\boldsymbol{R}_m} |\boldsymbol{R}_m\rangle \tag{4}$$

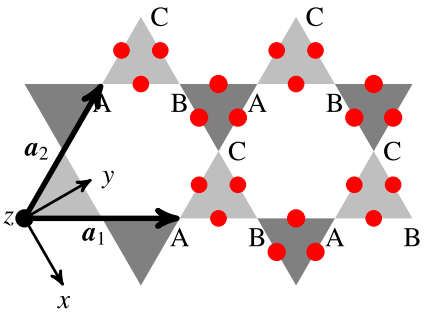

FIG. 1. (Color online) Kagome lattice with lattice vectors $\boldsymbol{a}_1$ and $\boldsymbol{a}_2$ in the xy plane. Identical atoms A, B, and C are placed at the corners of the triangles. Dzyaloshinskii-Moriya vectors are aligned normal to the lattice plane and are represented by red dots: along $+z$ ($-z$) for a counterclockwise (clockwise) chirality: A-B-C (C-B-A).

of $\mathcal{H}_{\mathrm{H}}$ are "one-magnon states"; they expose magnons as collective excitations because the spin deviation of $\hbar$ is distributed uniformly over all N spins. $\boldsymbol{R}_m$ is the vector pointing to lattice site m and $|\boldsymbol{R}_m\rangle$ denotes the state with all spins aligned along the ferromagnetic ground state except the one at lattice site m; its z component is reduced by $\hbar$.

The second contribution in Eq. (2),

$$\mathcal{H}_{\mathrm{DM}} = \sum_{m\neq n} \boldsymbol{D}_m^n(\hat{\boldsymbol{s}}_m \times \hat{\boldsymbol{s}}_n), \tag{5}$$

accounts for the antisymmetric Dzyaloshinskii-Moriya (DM) interaction [16,17]. $\boldsymbol{D}_m^n$ is the DM vector between sites m and n ($\boldsymbol{D}_m^n = -\boldsymbol{D}_n^m$).

For completeness, we introduce the coupling to an external magnetic field $\boldsymbol{H}$,

$$\mathcal{H}_{\mathrm{ext}} = -g\mu_{\mathrm{B}} \sum_n \boldsymbol{H}\cdot\hat{\boldsymbol{s}}_n. \tag{6}$$

g and μ_{B} denote the g factor of electrons and Bohr's magneton, respectively. For the problems treated in this study, this contribution is irrelevant; it is, however, needed in the description of the magnon Hall effect (e.g., Ref. [14]). Likewise, neither magnetocrystalline anisotropy nor magnon-magnon interaction are considered in this paper.

B. Berry curvature and Chern numbers

According to Moriya's symmetry rules [17], the DM vectors $\boldsymbol{D}_m^n$ are perpendicular to the kagome lattice, that is, they are aligned along the z direction. Their orientation is given by the chirality of the triangles in the kagome lattice: those with counterclockwise (clockwise) chirality point along $+z$ ($-z$) direction (cf. the red dots in Fig. 1).

Because of the DM interaction a magnon accumulates an additional phase upon propagation from site m to n (cf. the supplemental online material of Ref. [10]). This can be viewed as a result of a textured flux within the plaquettes of the kagome lattice [18], in analogy to the Haldane model for an electronic topological insulator [19]. Thus we are concerned with a nonzero Berry curvature $\boldsymbol{\Omega}(\boldsymbol{k})$ (Ref. [4]) and with topological invariants. Please note the difference to models for strongly correlated electrons on a kagome lattice with spin anisotropy, in which the Berry phase and the electronic edge modes are brought about by statically tilted spins [20].

For a given set of parameters $\{J_m^n, D_m^n\}$, we solve the eigenproblem for the Hamiltonian $\mathcal{H}$. From the computed eigenvectors $|i(\boldsymbol{k})\rangle$ and dispersion relations $\varepsilon_i(\boldsymbol{k})$ [wave vector $\boldsymbol{k} = (k_x, k_y)$, band index i] the Berry curvature

$$\boldsymbol{\Omega}_j(\boldsymbol{k}) \equiv \mathrm{i}\sum_{i\neq j} \frac{\langle i(\boldsymbol{k})|\nabla_{\boldsymbol{k}}\mathcal{H}(\boldsymbol{k})|j(\boldsymbol{k})\rangle \times \langle j(\boldsymbol{k})|\nabla_{\boldsymbol{k}}\mathcal{H}(\boldsymbol{k})|i(\boldsymbol{k})\rangle}{[\varepsilon_i(\boldsymbol{k}) - \varepsilon_j(\boldsymbol{k})]^2} \tag{7}$$

and the Chern numbers

$$C_j \equiv \frac{1}{2\pi}\int_{\mathrm{BZ}} \Omega_j^z(\boldsymbol{k})\, dk^2 \tag{8}$$

are calculated for each band j. We recall that these are determined solely by the magnonic band structure of the bulk.

C. Edge magnons

For investigating magnonic edge modes we consider a semi-infinite solid. Thereby, finite-size effects that show up in a slab (stripe) calculation are avoided; for example, hybridization of edge states at opposite edges could result in artificial band gaps.

The magnon band structure is analyzed in terms of the spectral density:

$$N_n(\varepsilon,\boldsymbol{k}) = -\frac{1}{\pi}\lim_{\eta\to 0^+} \mathrm{Im\ tr}\, G_{nn}(\varepsilon + \mathrm{i}\eta, \boldsymbol{k}) \tag{9}$$

for site n. The limit $\eta \searrow 0$ is not taken but $\eta = 0.005\,\mathrm{meV}$.

The blocks G_{nm} of the Green function of the semi-infinite system are computed by a renormalization technique [21] which is briefly sketched now. The system is decomposed into principal layers for which the exchange interaction is only among adjacent principal layers. Restricted to nearest- and next-nearest-neighbor interactions, the thinnest principal layers possible are shown in Fig. 2 for two different edges.

In terms of the principal layers, the blocks of the Green's matrix for the semi-infinite system fulfill

$$\delta_{nm} = \sum_{j=0}^{\infty}(z\,\delta_{nj} - H_{nj})\cdot G_{jm}, \quad n,m \geqslant 0, \tag{10}$$

where $z = \varepsilon + \mathrm{i}\eta$. The dimension of each block matrix is the number of basis atoms in a principal layer. The diagonal blocks H_{nn} comprise the intralayer interactions within the nth principal layer; in particular, H_{00} is the Hamilton matrix with interactions within the surface layer (red layer in Fig. 2 labeled "0th layer"). The interlayer couplings are comprised in $H_{n,n+1}$; for example, H_{01} is for the interaction between the surface layer and the subsurface layer (red and blue in Fig. 2). By construction of the principal layers, $H_{nm} = 0$ for $|n-m| \geqslant 2$.

From Eq. (10), one eliminates all blocks G_{nm} with odd principal-layer indices (e.g., the blue layers in Fig. 2); the result is an equation with identical form but with renormalized blocks H_{nm}. By repeating this elimination process, the interlayer interactions can iteratively be reduced ($||H_{nm}|| \to 0$). From the renormalized Hamilton matrix which is effectively block diagonal, we calculate the layer-diagonal Green-function

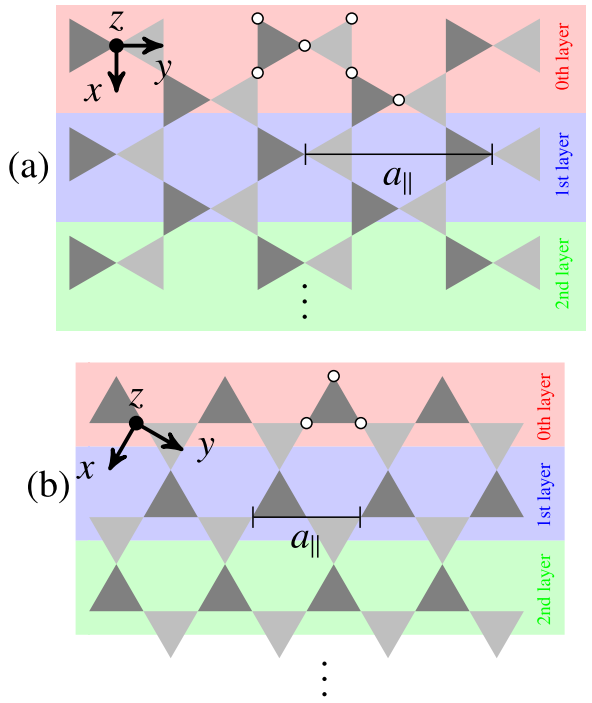

FIG. 2. (Color online) Edges of the kagome lattice. For two different terminations of the bulk system, (a) and (b), the semi-infinite lattice is divided into the thinnest principal layers possible if only nearest- and next-nearest-neighbor interactions are present. White dots show the basis consisting of six (a) and three (b) sites, respectively. The lattice constants $a_\parallel$ are indicated.

blocks by

$$G_{nn} = (z - H_{nn})^{-1}. \tag{11}$$

All other G_{nm} are accessible by transfer matrices.

III. RESULTS AND DISCUSSION

In the following analysis we assume a kagome lattice with all three basis atoms being identical, i.e., with identical spin and exchange parameters; an exception is Sec. III C. We consider the Heisenberg exchange between nearest (J_N) and next-nearest (J_{NN}) sites; the Dzyaloshinskii-Moriya parameters account only for nearest-neighbor interactions (D).

A. Bulk-boundary correspondence

As investigated recently [14], the kagome lattice with ferromagnetic ground state shows four topologically different phases, with variables J_{NN}/J_N and D/J_N. These phases are distinguished by the triple of Chern numbers (C_1,C_2,C_3) of the three magnon bulk bands (Fig. 3) [22]. Note that the phase diagram results from analyzing an infinite crystal (bulk).

We now consider semi-infinite systems by introducing an edge according to Fig. 2(a). The local spectral density $N_n(\varepsilon,\boldsymbol{k})$ is calculated for four different sets of parameters which put the system into the four different topological phases [Figs. 4(a)–4(d)]. More precisely, we chose $\{J_{NN}/J_N, D/J_N\} = \{0,1\}$, $\{\frac{1}{2},1\}$, $\{0.81,1\}$, and $\{1,1\}$, all of which are marked by the red dots in Fig. 3.

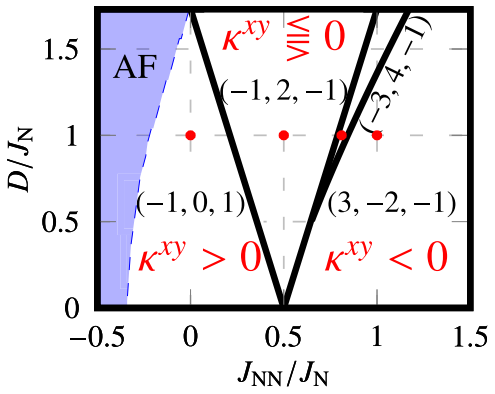

FIG. 3. (Color online) Topological phase diagram of the kagome lattice with regions characterized by sets (C_1,C_2,C_3) of Chern numbers. The antiferromagnetic (AF) phase is colored blue. Red dots mark those variable sets $\{J_{NN}/J_N, D/J_N\}$ for which local densities of states are calculated. The sign of the transverse thermal conductivity κ^{xy} of the magnon Hall effect is given in red; it is unique for the phases $(-1,0,1)$ and $(3,-2,-1)$.

The three magnon bulk bands are separated from each other by gaps generated by the Dzyaloshinskii-Moriya interaction. Topologically nontrivial edge modes are easily identified as bands that cross these band gaps and, thus, connect adjacent bulk bands. Furthermore, they are robust against variations of the exchange parameters at the edge. The edge states are singly degenerate and decay rapidly towards the bulk (Fig. 5). The atomic-layer-resolved spectral density clearly shows a localization of the edge state at the first 20 atomic layers (blue histogram in Fig. 5). The magnon edge resonance shows features up to the 300th atomic layer (green histogram in Fig. 5).

In contrast to electronic $\mathbb{Z}_2$ topological insulators—which rely on time-reversal invariance—magnonic edge modes do not occur in Kramers pairs. This is readily explained by the fact that a single spin orientation is present in the system (here: ferromagnetic ground state with spins along the $+z$ direction). We recall that time reversal changes the sign of $\boldsymbol{k}$ and reverses the spin orientation. A reversal of the spin orientation alters the signs of all Chern numbers, which has the consequence that the propagation direction of the topologically nontrivial edge modes is reversed as well. These "reversed" edge states can be regarded as the time-reversed (Kramers) partners in an electronic $\mathbb{Z}_2$ topological insulator.

The topological phase—specified by its set of Chern numbers—is of particular importance for the topologically nontrivial edge modes as it determines both their propagation direction and their number. This is the "bulk-boundary correspondence" [1,5,23]: a bulk property, i.e., the Chern numbers, dictates surface properties, i.e., the edge magnons. The sum of Chern numbers up to the ith band,

$$\nu_i \equiv \sum_{j\leqslant i} C_j, \tag{12}$$

is the "winding number" of the edge states in band gap i (cf. Refs. [5] and [23]). In other words, $|\nu_i|$ is the number of topologically nontrivial edge states in the ith band gap; their propagation direction is given by $\mathrm{sgn}(\nu_i)$. We emphasize that

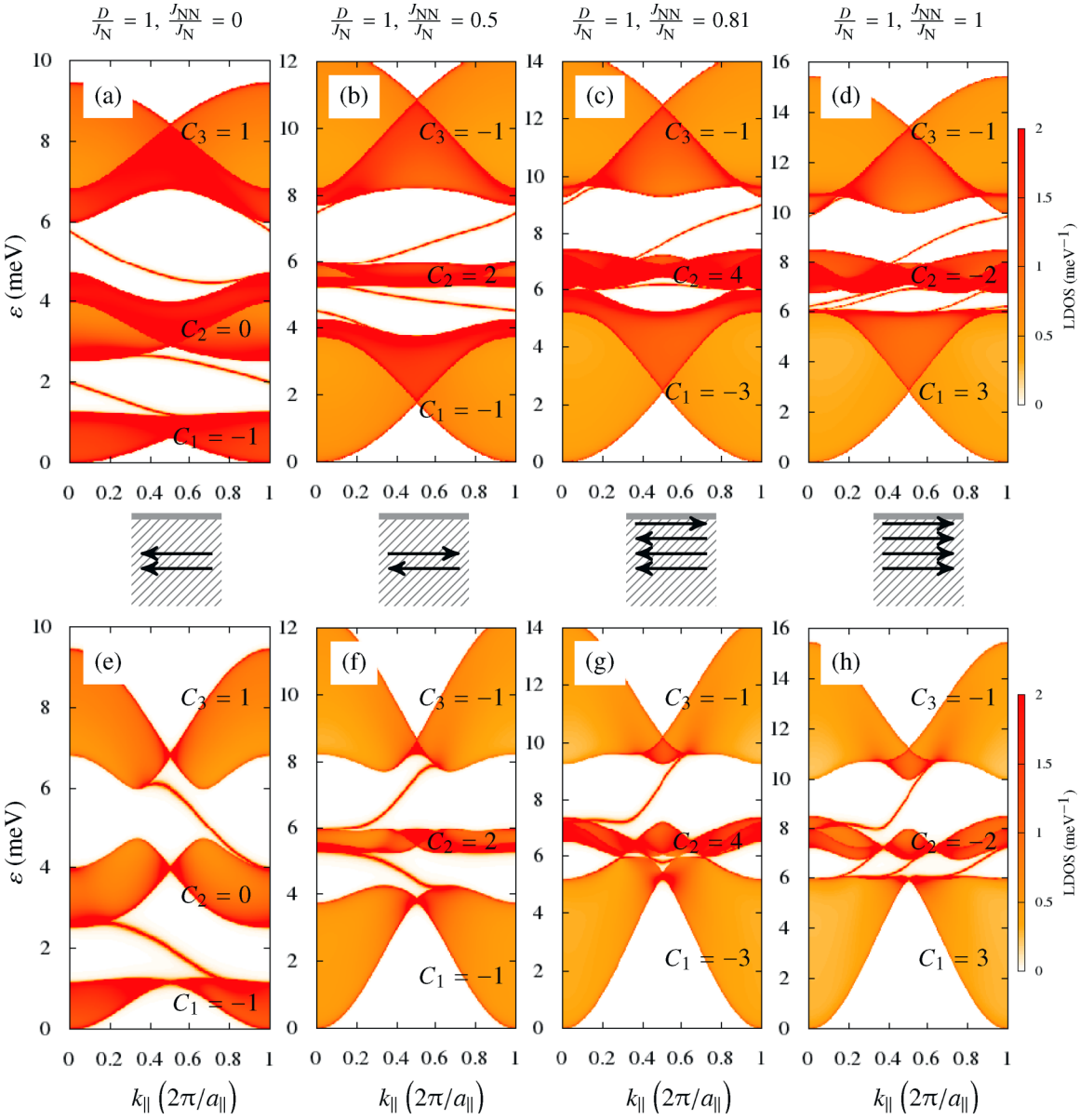

FIG. 4. (Color online) Edge magnons in a kagome lattice. The spectral density of states of an edge site is shown as color scale ["local density of states" (LDOS), right] for the edge geometries of Fig. 2(a) [top row, (a)–(d)] and Fig. 2(b) [bottom row, (e)–(h)] in the entire edge Brillouin zone. Bulk magnons appear as extended regions separated by band gaps ("projected bulk band structure"), while edge magnons bridge these band gaps. The topological phases are characterized by their bulk-band-resolved Chern numbers C_i ($i = 1,2,3$) given in each panel; the respective exchange parameters are given as well ($J_N = 1$ meV). The topologically nontrivial edge magnon modes and their propagation direction are sketched in the central row.

the geometry of the edge is irrelevant for these fundamental features.

We illuminate the above rule by considering as an example the topological phase $(-1,2,-1)$. For both edge geometries [Figs. 4(b) and 4(f)], there is a single nontrivial edge mode with negative dispersion (slope) within the lowest energy gap because $\nu_1 = C_1 = -1$. In the second band gap there is a single edge mode with positive dispersion, in accordance with $\nu_2 = C_1 + C_2 = 1$. Because the sum over all Chern numbers vanishes—$\nu_n = \sum_i^n C_i = 0$, where $n = 3$ is the total number of bands—there are never topological nontrivial edge states above the uppermost band. These relations hold also for the other topological phases, as is evident from the other panels of Fig. 4.

B. Edge modes and magnon Hall effect

The magnon Hall effect (MHE) is a transverse heat current upon application of a temperature gradient which was discovered for the ferromagnetic insulator $Lu_2V_2O_7$ by Onose *et al.* (Ref. [10]). The pyrochlore $Lu_2V_2O_7$ consists of stacked two-dimensional kagome lattices separated by an additional monatomic layer. Matsumoto and Murakami explained the MHE by uncompensated magnon edge currents

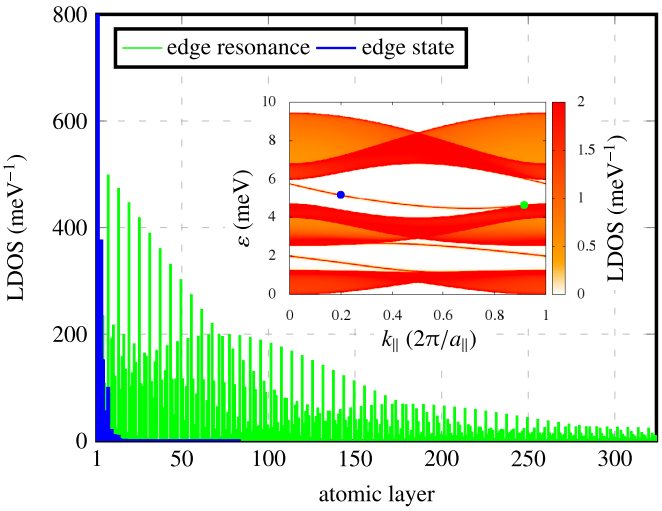

FIG. 5. (Color online) Edge localization of magnons. The site-resolved spectral density ("LDOS") is shown versus layer index (edge = layer 1) for an edge magnon [blue; the respective $(\varepsilon,\boldsymbol{k})$ is marked by the blue dot in the inset] and an edge resonance (green; cf. the green dot in the inset). $D/J_\mathrm{N} = 1$, $J_\mathrm{NN}/J_\mathrm{N} = 0$, and $J_\mathrm{N} = 1$ meV, as in Fig. 4(a).

in two dimensions [11,12]. The intrinsic contribution to the transverse thermal conductivity,

$$\kappa^{xy} = -\frac{k_\mathrm{B}^2 T}{(2\pi)^2\hbar}\sum_i \int_\mathrm{BZ} c_2(\varrho_i)\,\Omega_i^z(\boldsymbol{k})\,dk^2, \qquad (13)$$

is intimately related to the Chern numbers defined in Eq. (8). The sum runs over all bands i in the magnon dispersion relation, and the integral is over the Brillouin zone (BZ). The energy- and temperature-dependent Bose distribution function ϱ_i enters the function

$$c_2(x) \equiv (1+x)\left(\ln\frac{1+x}{x}\right)^2 - (\ln x)^2 - 2\,\mathrm{Li}_2(-x). \qquad (14)$$

Li_2 is the dilogarithm.

The magnon Hall effect in kagome lattices has extensively been discussed in Ref. [14]. In particular, the sign of κ^{xy} has been shown to depend on the topological phase of the bulk system. In that publication, an explanation was given by means of Chern numbers and a high-temperature limit of κ^{xy}. However, this dependence can be understood in terms of edge modes and their propagation direction as well, as we will show in the following.

In the phase $(-1,0,1)$ there are two topologically nontrivial edge modes, both with negative dispersion [Figs. 4(a) and 4(e)]. As a consequence, heat transport can only proceed in one direction which is towards the left, as sketched in the center row of Fig. 4. Likewise, the phase $(3,-2,-1)$ shows four edge modes, all of which with positive dispersion; thus the heat transport is towards the right [panels (d) and (h)]. Because all nontrivial edge modes propagate in the same direction, the sign of the thermal Hall conductivity is fixed within these topological phases; its sign does not depend on the temperature.

The other two phases, $(-1,2,-1)$ and $(-3,4,-1)$, support edge modes of both propagation directions [panels (b), (c), (f), and (g) in Fig. 4]. Thus the sign of κ^{xy} depends on the occupation probability of the edge magnons, that is, on temperature. At low temperatures, edge modes in the first band gap are more occupied than edge modes in the second band gap. Thus the heat transport is dominated by the former edge modes; here: towards the left. Upon increasing the temperature, the edge modes in the second band gap become increasingly populated, with the consequence that the heat current is mainly mediated by these magnons, provided that the absolute values of their velocities are larger than those of the magnons in the first band gap; hence it is toward the right. This finding—a change of sign in κ^{xy} with temperature—is in full agreement with the analysis in Ref. [14].

C. Hybridization of edge modes

Topologically nontrivial edge magnons are protected by symmetry because their existence is dictated by the topology of the bulk system. However, their detailed dispersion relation may change under perturbations, for example, surface relaxation and reconstruction as well as adsorption of magnetic sites. All these modifications alter the exchange parameters at the edge with respect to those of the bulk. In the following, we account for such effects by changing the interaction parameters J_N within the very first principal layer but keeping the bulk parameters constant ($D/J_\mathrm{N} = 0.1$).

It turns out that even for the ideal (unperturbed) edge there exists a trivial edge mode in the second band gap, close to the wedge-shaped region at $k_\parallel = 0.5 \times 2\pi/a_\parallel$ and $\varepsilon \approx 5.3$ meV [Fig. 6(a)]. For increasing $J_\mathrm{N}^\mathrm{edge}$ this trivial mode is shifted towards higher energies [(b)–(d)]. Eventually, it hybridizes with the topologically nontrivial mode (d).

This hybridization of trivial with nontrivial edge modes shows severe consequences for the topologically nontrivial edge state. For the ideal edge, it connects the third with the second bulk band within a $k_\parallel$ range of less than one edge Brillouin zone. More precisely, it "leaves" the third bulk band at about $k_\parallel = 0.3 \times 2\pi/a_\parallel$ and "enters" the second bulk band at about $0.8 \times 2\pi/a_\parallel$ [Fig. 6(a)]. In the case of hybridization, however, this period is enlarged by $2\pi/a_\parallel$, that is by the entire extension of one Brillouin zone [Fig. 6(d)]. The periodicity of the band structure remains unchanged with $2\pi/a_\parallel$, as is obvious within an extended zone scheme.

The effect of hybridization on the periodicity of the edge states can be understood by making use of the periodicity of the Brillouin zone. By identifying $k_\parallel = 0$ and $k_\parallel = 2\pi/a_\parallel$ the edge Brillouin zone becomes a cylinder (Fig. 7). Within this representation bulk bands form broad rings encircling the cylinder's surface. In the systems of Fig. 6 two edge modes show up. The topologically nontrivial mode corresponds to the blue thread in Fig. 7(a) labeled "nontrivial edge mode." By twisting the cylinder (i.e., rotation of its top or bottom) the nontrivial mode is continuously transformed into a line parallel to the rotational axis of the cylinder. However, the trivial mode [green thread in Fig. 7(a) labeled "trivial edge mode"] forms a closed loop around the cylinder's surface and, therefore, will not change under twisting.

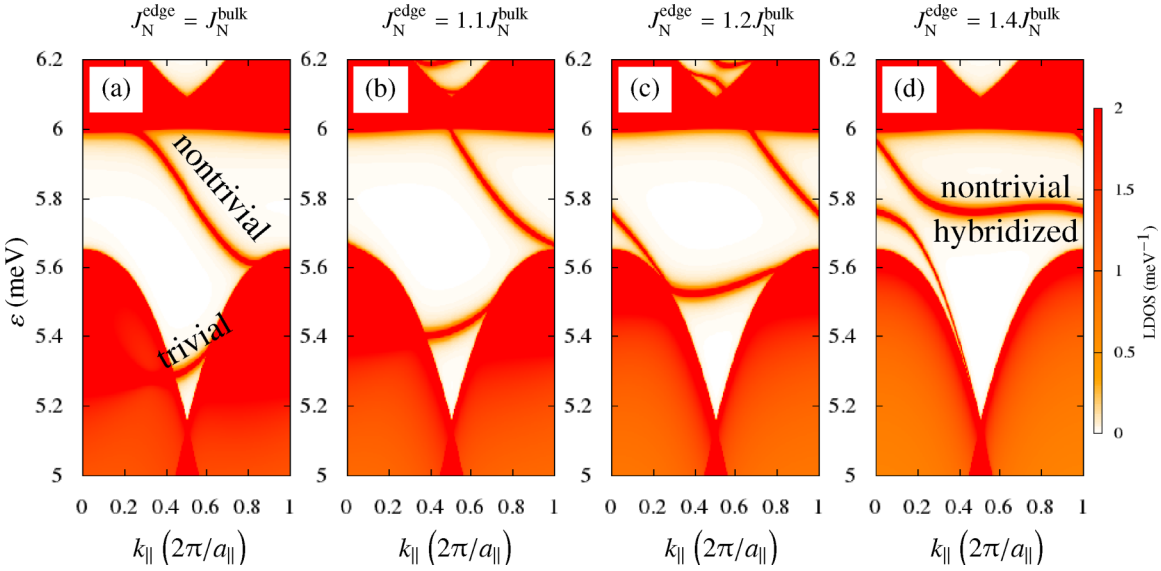

FIG. 6. (Color online) Hybridization of a topologically nontrivial with a trivial edge magnon. The local density of states (LDOS) for the edge geometry of Fig. 2(a) is shown as a color scale for several exchange parameters of the edge sites [(a)–(d); as indicated at the top of each panel]. $D/J_N = 0.1$, $J_N = 1$ meV, and $J_{NN} = 0$.

For the unperturbed edge [Fig. 6(a)] the trivial mode is located at a lower energy than the nontrivial mode; it is concealed almost entirely by the lower bulk band. For increasing perturbation J_N^{edge}, this trivial mode is shifted towards higher energies and, eventually, approaches the energy range covered by the nontrivial mode. Thus the topologically trivial and nontrivial mode hybridize with each other [red thread labeled "nontrivial hybridized edge mode" in Fig. 7(b)]. As a result, a nontrivial edge mode is formed that not only connects the two bulk bands but also encircles the cylinder's surface for another entire circulation; an additional extension of the Brillouin zone $(2\pi/a_\parallel)$ is necessary to traverse the band gap. Mathematically the hybridization can be understood as a Dehn twist [24] applied to the cylinder about the trivial mode modifying the nontrivial mode. As Dehn twists are self-homeomorphisms the topology of the cylinder stays untouched. We note in passing that a further increase of J_N^{edge} shifts the trivial edge mode into the upper bulk band and the original nontrivial mode with simple periodicity is recovered.

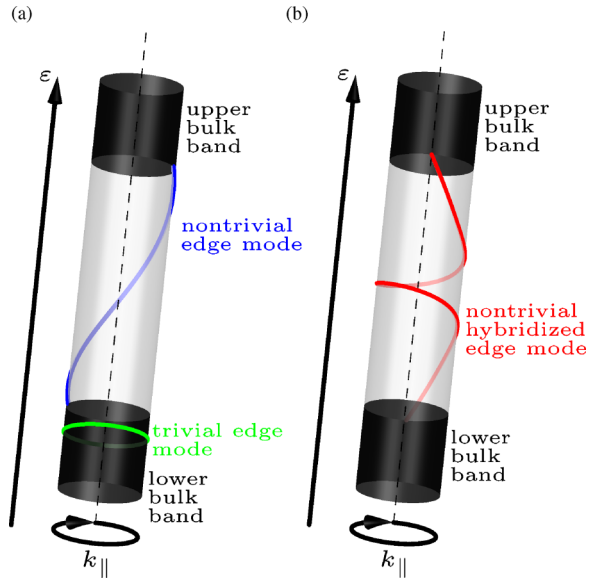

FIG. 7. (Color online) Topology and hybridization of a topologically nontrivial with a trivial edge magnon. Cylinder representation of a system with two bulk bands (black). The dashed line indicates the "seam" at $k_\parallel = 0 = 2\pi/a_\parallel$. (a) Sketch of the band structure in Fig. 6(a). Trivial edge modes (green) circle around the cylinder; nontrivial edge modes (blue) connect the bulk bands. The trivial modes' energy is not located within the energy range of the nontrivial mode. (b) Sketch of the band structure in Fig. 6(d). A hybridization of a trivial and nontrivial edge mode generates a nontrivial mode circulating the cylinder (red).

The above argumentation is readily generalized: if a nontrivial mode hybridizes with n trivial modes, its period is increased by $n \times 2\pi/a_\parallel$ since n Dehn twists are applied. In any case, the resulting mode is always nontrivial due to its topology determined by the bulk. Therefore, a twisting of the cylinder will always transform the hybridized mode into a line parallel to the cylinder's rotational axis.

A similar hybridization has been observed in electronic topological insulators: for Bi_2Te_3 covered by a monolayer of Au, the Dirac surface state of Bi_2Te_3 hybridizes with sp states of Au (Ref. [25]), thereby increasing its period in full analogy to the magnon case presented here.

IV. OUTLOOK

Having analyzed in detail the topology of edge modes in kagome lattices, it is obvious to extend such an investigation to three-dimensional systems, especially to ferromagnetic insulators with pyrochlore structure.

Our investigation of the edge modes in kagome systems calls for experimental verification. The dispersion relation could be mapped by spin-polarized electron energy loss

spectroscopy (SPEELS) [26] or time-resolved spectroscopies [27]. Within this respect, materials with different topological phases are desirable, for example, $Lu_2V_2O_7$ with positive and $In_2Mn_2O_7$ with negative thermal Hall conductivity [28]; these should exhibit nontrivial surface modes with opposite slope of the dispersion.

Recently, Matsumoto, Shindou, and Murakami derived a theory of the thermal Hall effect in magnets with dipolar interaction and in antiferromagnets [29]. In such systems, pairs of edge states could occur that can be regarded as time-reversed partners of each other, which calls for their detailed investigation.

[1] H. Hasan and C. Kane, Rev. Mod. Phys. **82**, 3045 (2010).
[2] X.-L. Qi and S.-c. Zhang, Rev. Mod. Phys. **83**, 1057 (2011).
[3] M. Z. Hasan and J. E. Moore, Annu. Rev. Condens. Matter Phys. **2**, 55 (2011).
[4] M. V. Berry, Proc. R. Soc. A **392**, 45 (1984).
[5] Y. Hatsugai, Phys. Rev. Lett. **71**, 3697 (1993).
[6] D. Xiao, M.-C. Chang, and Q. Niu, Rev. Mod. Phys. **82**, 1959 (2010).
[7] C. Strohm, G. L. J. A. Rikken, and P. Wyder, Phys. Rev. Lett. **95**, 155901 (2005).
[8] L. Zhang, J. Ren, J.-S. Wang, and B. Li, Phys. Rev. Lett. **105**, 225901 (2010).
[9] L. Zhang, J. Ren, J.-S. Wang, and B. Li, J. Phys. Condens. Matter **23**, 305402 (2011).
[10] Y. Onose, T. Ideue, H. Katsura, Y. Shiomi, N. Nagaosa, and Y. Tokura, Science **329**, 297 (2010).
[11] R. Matsumoto and S. Murakami, Phys. Rev. Lett. **106**, 197202 (2011).
[12] R. Matsumoto and S. Murakami, Phys. Rev. B **84**, 184406 (2011).
[13] L. Zhang, J. Ren, J.-S. Wang, and B. Li, Phys. Rev. B **87**, 144101 (2013).
[14] A. Mook, J. Henk, and I. Mertig, Phys. Rev. B **89**, 134409 (2014).
[15] W. Heisenberg, Z. Phys. **49**, 619 (1928).
[16] I. Dzyaloshinsky, J. Phys. Chem. Solids **4**, 241 (1958).
[17] T. Moriya, Phys. Rev. **120**, 1 (1960).
[18] H. Katsura, N. Nagaosa, and P. A. Lee, Phys. Rev. Lett. **104**, 066403 (2010).
[19] F. D. M. Haldane, Phys. Rev. Lett. **61**, 2015 (1988).
[20] K. Ohgushi, S. Murakami, and N. Nagaosa, Phys. Rev. B **62**, R6065(R) (2000).
[21] J. Henk and W. Schattke, Comput. Phys. Commun. **77**, 69 (1993).
[22] The Chern numbers have been defined with opposite sign in Ref. [14]. In this paper, the definition of the Berry curvature yields a sign of the thermal Hall conductivity, Eq. (13), in agreement with Refs. [11] and [12].
[23] Y. Hatsugai, Phys. Rev. B **48**, 11851 (1993).
[24] M. Dehn, Acta Math. **69**, 135 (1938).
[25] F. Muñoz, J. Henk, and I. Mertig (unpublished).
[26] K. Zakeri, Y. Zhang, T.-H. Chuang, and J. Kirschner, Phys. Rev. Lett. **108**, 197205 (2012).
[27] S. O. Demokritov and B. Hillebrands, in *Spin Dynamics in Confined Magnetic Structures*, edited by B. Hillebrands and K. Ounadjela, Topics in Applied Physics (Springer, Berlin, 2002), Chap. 3, p. 65.
[28] T. Ideue, Y. Onose, H. Katsura, Y. Shiomi, S. Ishiwata, N. Nagaosa, and Y. Tokura, Phys. Rev. B **85**, 134411 (2012).
[29] R. Matsumoto, R. Shindou, and S. Murakami, Phys. Rev. B **89**, 054420 (2014).